ACS APPLIED ENERGY MATERIALS

www.acsaem.org Article

Boron Spin-On Doping for Poly-Si/SiO$_x$ Passivating Contacts

Zetao Ding,[⊥] Thien N. Truong,[*,⊥] Hieu T. Nguyen, Di Yan, Xinyu Zhang, Jie Yang, Zhao Wang, Peiting Zheng, Yimao Wan, Daniel Macdonald, and Josua Stuckelberger*

Cite This: ACS Appl. Energy Mater. 2021, 4, 4993–4999

Read Online

ACCESS | Metrics & More | Article Recommendations

ABSTRACT: Herein, we fabricate and characterize p-type passivating contacts based on industrial intrinsic polycrystalline silicon (poly-Si)/thermal-SiO$_x$/n-type crystalline Si (c-Si) substrates using a spin-on doping technique. The impacts of drive-in temperature, drive-in dwell time, and intrinsic poly-Si thickness on the boron-doped poly-Si passivating contacts are investigated. First, the contact passivation quality improves with an increasing thermal budget (<950 °C) but then decreases again for excessive thermal annealing (>950 °C). Second, the thickness of the intrinsic poly-Si film shows only a little impact on the performance. After a hydrogenation treatment by depositing an AlO$_x$/SiN$_x$ stack and subsequent annealing in forming gas, the optimized poly-Si passivating contacts show an implied open-circuit voltage (iV_{oc}) > 720 mV, together with a contact resistivity (ρ_c) below 5 mΩ cm^2. These results demonstrate that boron spin-on doping is a promising alternative to the conventional BBr_3 thermal diffusion for the fabrication of p-type poly-Si passivating contacts.

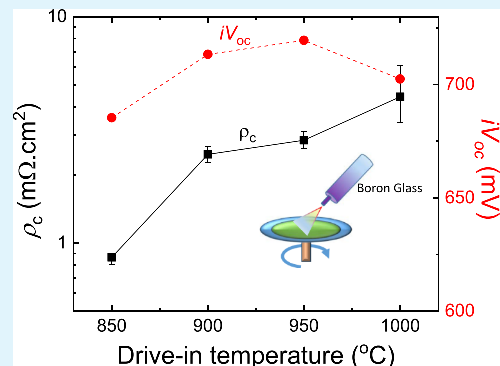

KEYWORDS: *passivating contact, poly-Si, boron, spin-on doping, TOPCon, POLO, silicon solar cells*

Downloaded via AUSTRALIAN NATL UNIV on January 31, 2023 at 23:37:54 (UTC).
See https://pubs.acs.org/sharingguidelines for options on how to legitimately share published articles.

1. INTRODUCTION

Polycrystalline silicon (poly-Si)-based passivating contacts are an established technology for high-performance silicon solar cells, with many groups reporting light-to-electricity efficiencies of >25%, thanks to a low carrier recombination current density (J_0) of less than 5 fA/cm^2 and a contact resistivity (ρ_c) on the order of 1 mΩ cm^2.[1−10] Furthermore, the poly-Si passivating contact has a higher temperature stability than Si heterojunction structures, making it compatible with existing high-temperature industrial processes.[11−14]

The doping of poly-Si passivating contacts can be categorized into two approaches: *in situ* and *ex situ* doping. The former approach utilizes the deposition process to incorporate dopants into Si films at the same time, followed by an annealing step.[15−20] Disadvantages of this approach are the complexity in controlling various parameters of the deposition and annealing and the inclusion of dangerous and toxic gases (*e.g.*, phosphine and boron tribromide) which require additional safety measures. The latter approach, *ex situ* doping, separates the deposition and doping processes, making the optimization of each process easier.[21−26] Among the *ex situ* doping methods, liquid dopant-based doping,[27−35] specifically spin-on glass, has shown several unique advantages compared to gas diffusion and ion implantation doping. First, dopant-containing solutions are less toxic, hence reducing extra safety measures often seen in the gas diffusion[36] or ion implantation processes.[37] Also, the dopant-containing liquids can be applied on patterned regions easily without shadow masks through printing technologies.[38,39] Besides, the solutions can convey diverse dopant species of different concentrations at the same time, which enhances the versatility of the doping processes.

In our previous work,[31] we demonstrated that phosphorus spin-on doping can be an effective alternative doping method to the conventional $POCl_3$ diffusion in n-type poly-Si passivating contacts' fabrication. In this work, the effects of annealing temperature, drive-in time, and poly-Si film thickness on the performance of spin-on boron-doped p-type passivating contacts will be investigated. Based on the optimal processing parameters obtained from these studies, we demonstrate that boron spin-on doping could be employed as a new and promising doping method for poly-Si/SiO$_x$ passivating contacts.

2. EXPERIMENTAL DETAILS

The experimental process flow is described in Figure 1. Industrially planarized n-type (100)-oriented Czochralski wafers with a base resistivity of 5.5 ± 0.4 Ω cm and a thickness of 164 ± 3 μm were used for all experiments. Following an industrial saw damage etch and wafer cleaning step, a thermal oxidation process at 700 °C for 5 min

Received: February 22, 2021
Accepted: April 20, 2021
Published: April 28, 2021

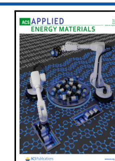

© 2021 American Chemical Society

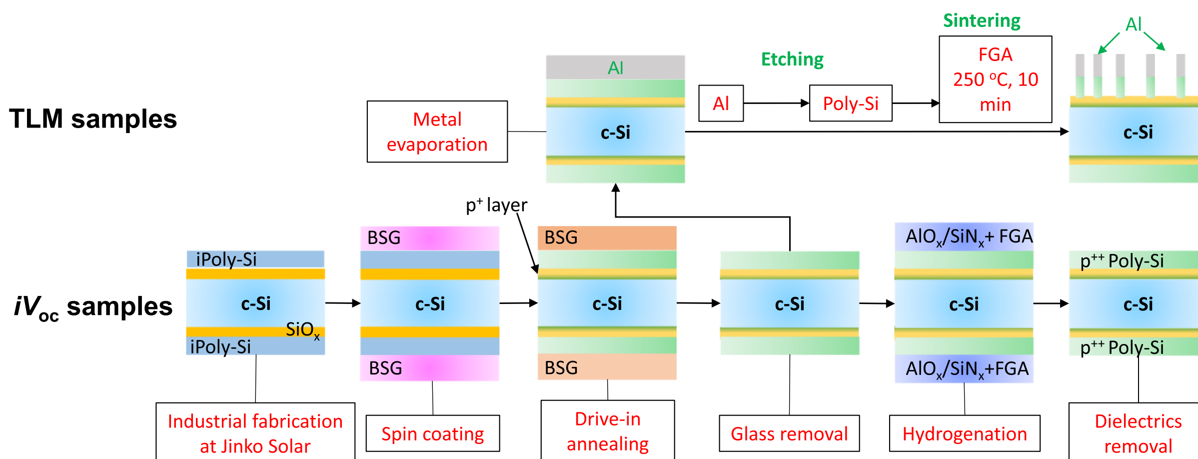

Figure 1. Flowchart of the experimental processes.

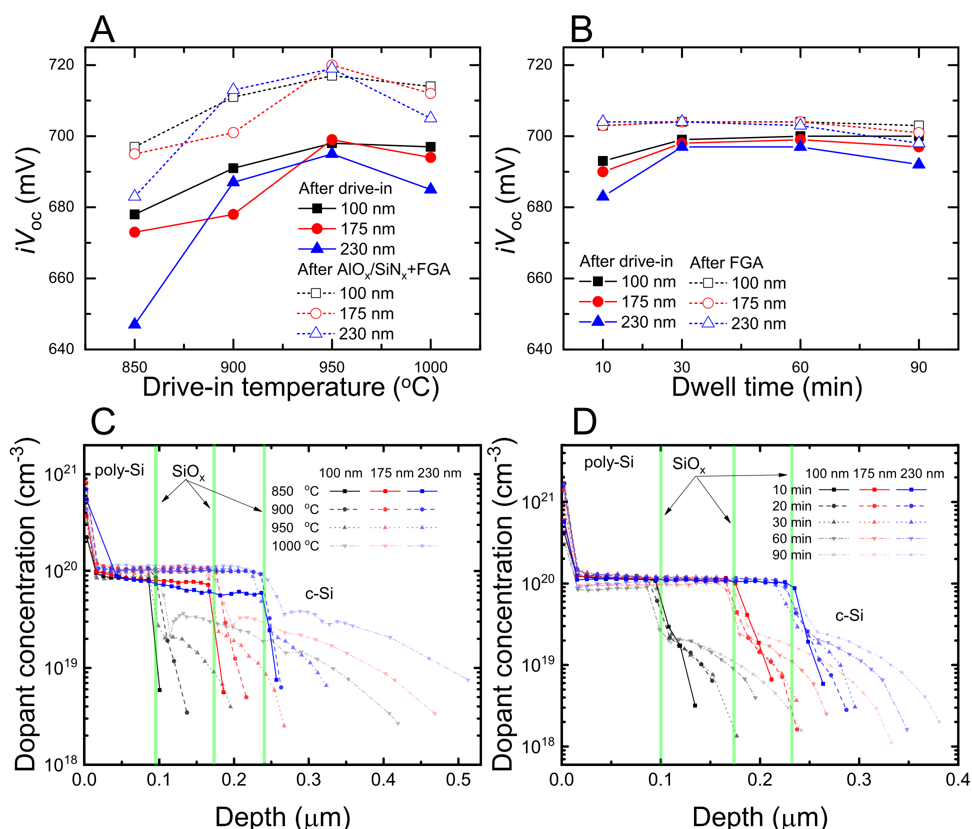

Figure 2. Implied open-circuit voltage (iV_{oc}) and electrically active boron profiles of different poly-Si samples (A,C) annealed at different temperatures for 60 min and (B,D) annealed at 950 °C for different dwell times, respectively, before and after hydrogen treatments (ECV measured before hydrogenation). Locations of the SiO_x layers vary with thicknesses of the poly-Si films, as denoted by green vertical lines in (C,D). The iV_{oc} value was measured using a PCD (QSSPC) technique in the transient mode at 1 sun intensity.

was performed in pure oxygen to form an ultrathin (<2 nm) silicon oxide (SiO_x) layer on both sides of the substrate. Subsequently, intrinsic poly-Si layers with different thicknesses (100, 175, and 230 nm) were deposited on top of the oxide layers using an industrial low-pressure chemical vapor deposition (LPCVD) system. These depositions were performed by Jinko Solar using their industrial scale tools. The thickness of the poly-Si layers was measured by an ellipsometer (J.A. Woollam ESM-300) using focusing probes. Before the spin-on doping process, the symmetric LPCVD poly-Si/SiO_x/Si samples were cleaned by a standard RCA procedure. A boron-containing spin-on glass layer (B-1500, [B] 7.2 × 10^{21} cm^{-3}, Desert Silicon) was spin-coated on both sides of these substrates using a spin coater (Laurell WS-650-23NPPB). The samples were then soft-baked at 90 °C for 10 min in a furnace and hard-baked at 200 °C for 6 min on a hot plate. The average thickness of spin-on glass layers in this experiment is ∼115 nm, which was measured by the focused ellipsometer on polished sister samples using the Cauchy models for SiO_2. Next, to drive and activate the dopants into the poly-Si films and the underlying wafer, annealing steps with N_2 in a quartz tube furnace were performed at various temperatures and dwell times. The drive-in temperature was varied from 850 to 1000 °C for 60 min, and the drive-in dwell time was varied from 10 to 90 min at 950 °C. Subsequently, the silica glass layers were removed by dipping the samples in a diluted 3% HF solution. Finally, the samples were

https://doi.org/10.1021/acsaem.1c00550
ACS Appl. Energy Mater. 2021, 4, 4993−4999

hydrogenated by depositing a ~20 nm thermal-assisted atomic-layer-deposited AlO_x:H layer covered by a ~50 nm plasma-enhanced chemical-vapor-deposited SiN_x:H layer, and/or annealed in forming gas (FGA, 5% H_2, 95% Ar) at 425 °C for 30 min. For contact resistivity measurements, another set of samples, which had gone through the same processes as those described above, received a single-side coating of 300 nm of Al. Subsequently, a photolithography step was used to define transfer length method (TLM) contacts on the poly-Si surface, and Al in the non-contact area was etched using a mixture of phosphoric acid, nitric acid, and deionized (DI) water. The poly-Si films uncovered by the metal contacts were removed using an etching solution of tetramethylammonium hydroxide, isopropanol, silicic acid, and DI water. Care was taken during the etching process to fully remove the poly-Si layer between the metal pads while stopping at the interfacial SiO_x, leaving the buried shallow diffused doped region in the wafer intact. Finally, the samples were sintered in forming gas at 250 °C for 10 min before the contact resistivity measurements. The contact resistivity for each drive-in temperature was obtained by averaging the values from a set of four different samples fabricated at the same condition. The maximum and minimum of the error bars were determined by the maximum and minimum variations of the measured data.

A Sinton WCT-120 lifetime tester based on the photoconductance decay (PCD) method in the transient mode was used to measure the resulting implied open-circuit voltage (iV_{oc}) values at 1 sun before and after the hydrogenation process (AlO_x/SiN_x + FGA). The Kane−Swanson method[40] was used to extract the recombination current density (J_0) from the PCD results at a minority carrier density of 5×10^{15} cm^{-3}. The J_0 values were divided by 2 to represent the single-side recombination. The electrically active dopant profiles were measured by an electrochemical capacitance−voltage (ECV) setup (WEP Wafer Profiler CVP21). Based on the doping profiles, the Auger recombination current density ($J_{0,Aug}$) of the diffused part in the c-Si substrates can be calculated *via* the EDNA2 software[41] following the procedure described in ref 19. This allows us to separate the total J_0 into contributions of the Auger recombination, the lower threshold for J_0, in comparison with the recombination at the poly-Si/SiO_x/wafer interface, which is dependent on the surface (interface) recombination velocity. Different sheet resistance values were obtained using four-point probe (4PP) measurements, integrating the doping profiles, in combination with the contact resistivity by the TLM. There are differences in the values simulated by EDNA2 and those measured by the 4PP and TLM. This is due to the fact that, as in the 4PP method, the current flows from one probe, through the poly-Si and SiO_x films, to the other probe. In the TLM as well as simulated results from EDNA2, the translational conduction only occurs in the diffused c-Si film as the non-contacted poly-Si layer has already been removed.

3. RESULTS AND DISCUSSION

First, we investigate the effects of drive-in temperature and drive-in dwell time on the performance of the poly-Si/SiO_x passivating contacts with various poly-Si film thicknesses (100, 175, and 230 nm). The implied open-circuit voltage (iV_{oc}) reflects the passivation quality of the passivating contacts. Four different drive-in temperatures (850−1000 °C) with a fixed annealing time of 60 min are presented. Additionally, the dwell time at a fixed 950 °C annealing temperature was varied between 10 and 90 min. Figure 2 shows the iV_{oc} from samples with different poly-Si film thicknesses (100 nm as black, 175 nm as red, and 230 nm as blue color) as a function of the annealing temperature (A) and for different dwell times (B) before (filled symbols, solid lines) and after hydrogen treatments (open symbols, dashed lines). As can be seen from Figure 2A, all of the as-annealed samples show increased iV_{oc} with increasing annealing temperatures, reaching their highest values of ~690 mV at 950 °C. Further increasing the annealing temperature (>950 °C) results in a decrease in iV_{oc}. A similar trend is observed after a hydrogen treatment *via* AlO_x/SiN_x stacks and subsequent annealing in forming gas at 425 °C for 30 min.[42−44] After the hydrogenation, the iV_{oc} values increase to ~720 mV at 950 °C. This indicates that 950 °C is likely to be the optimal drive-in temperature for all of the poly-Si samples with thicknesses of 100−230 nm. Interestingly, decreasing drive-in annealing temperatures (<950 °C) show a larger variation in iV_{oc} of different poly-Si thicknesses. The trend observed in this work agrees well with those of other studies on *ex situ* B diffusion using BBr_3 sources.[45]

Figure 2B shows the iV_{oc} values from various poly-Si thicknesses (100 nm: black, 175 nm: red, and 230 nm: blue) as a function of drive-in dwell time (ranging from 10 to 90 min) at 950 °C before and after a hydrogen treatment by annealing in forming gas at 425 °C for 30 min (solid and dashed lines, respectively). Please note that here only molecular hydrogenation *via* FGA is applied in contrast to the atomic hydrogenation *via* the AlO_x/H/SiN_x/H stack for the variation of annealing temperatures in Figure 2A. Compared to the drive-in temperature case, the drive-in dwell time shows less influence on iV_{oc} (with ΔiV_{oc} ~10 mV) for different poly-Si thicknesses and before and after FGA. Longer drive-in dwell time results in increasing iV_{oc} for all thicknesses of the as-annealed samples, reaching an optimal dwell time of ~60 min, and then iV_{oc} begins to decrease upon further prolongation of drive-in dwell time, except for the thinnest poly-Si sample (100 nm, Figure 2B), where it continues to increase. A short annealing time possibly does not drive enough dopants into the substrates; meanwhile, a long dwell time introduces more dopants into the c-Si substrate. In fact, the higher doping concentration in the bulk of c-Si results in higher Auger recombination in the diffused part, which will likely reduce the performance of the passivating contacts. After forming gas annealing, all samples, regardless of their thickness, show a similar and improved iV_{oc} (~705 mV) when annealed for not longer than 60 min, compared to the non-hydrogenated samples. Meanwhile, on the prolonged-dwell-time samples (≥60 min), the improvements after FGA are minimal (ΔiV_{oc} <5 mV). It is worth noting here that the improvement after FGA is less pronounced than that obtained when using AlO_x/SiN_x + FGA, as reported in other studies.[42,46]

To verify our observations from the PCD measurements, doping profiles of the spin-coated samples were measured using the ECV method, as shown in Figure 2C,D. The concentration of boron inside the poly-Si layers is relatively uniform (~10^{20} cm^{-3}) for the samples annealed at temperatures ≥900 °C. Meanwhile, for the annealing temperature of 850 °C, we observe a significantly lower concentration of boron in the poly-Si film (~$5-8 \times 10^{19}$ cm^{-3}). The location of the oxide layer is identified by a steep drop in the concentration of boron (illustrated by a green stripe, Figure 2C,D). Higher annealing temperatures, as well as longer dwell times, show higher in-diffusion rates of boron into the c-Si substrate (Figure 2C,D). This may lead to the formation of more defects at the SiO_x/c-Si interface upon driving-in at higher temperatures and for longer time. On the other hand, a longer drive-in time will diffuse more dopants into the c-Si substrate, while the doping level in the poly-Si film remains almost unchanged regardless of the poly-Si thickness (Figure 2D). Therefore, it suggests that the iV_{oc} variation is dominated by dopant activation and in-diffusion into the c-Si substrate.

https://doi.org/10.1021/acsaem.1c00550
ACS Appl. Energy Mater. 2021, 4, 4993−4999

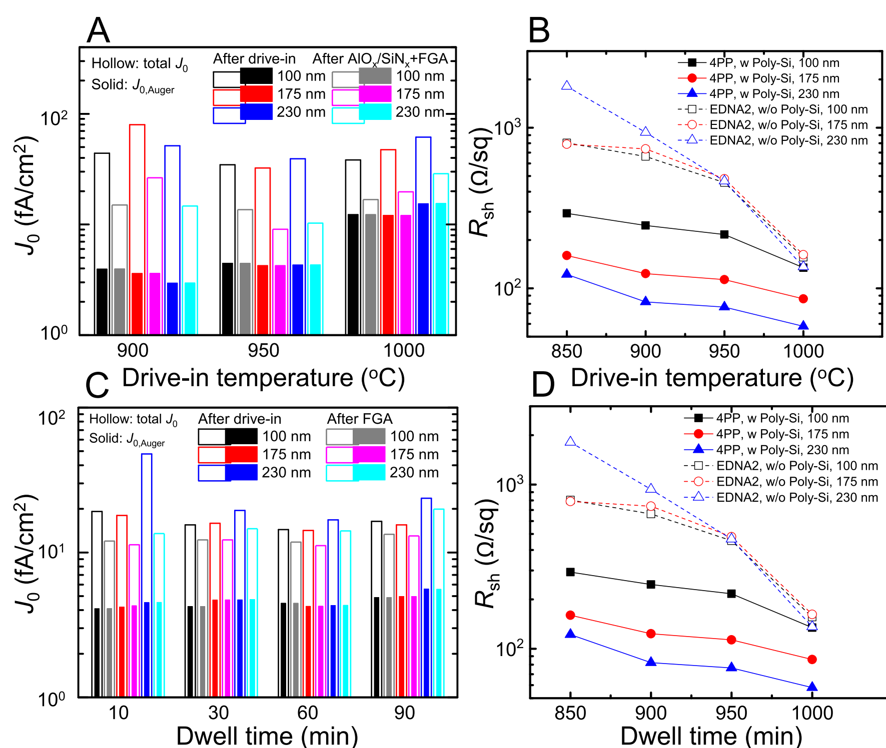

Figure 3. (A,C) Recombination current density (J_0) before and after a hydrogenation step by AlO_x/SiN_x + FGA (A) or FGA only (C) of different boron spin-on doped poly-Si/SiO_x/c-Si samples annealed at different temperatures for 60 min (A) and annealed at 950 °C for different dwell times (C), respectively. The hollow columns are the measured total J_o, whereas the solid columns represent the simulated contribution of the Auger recombination using EDNA2.[41] (B,D) Corresponding sheet resistance of the samples including the doped poly-Si layer, measured by a 4PP and the simulated R_{sh} by EDNA2 using only the diffused doping concentration in the c-Si substrate.

Next, we investigate the effects of the drive-in temperature and dwell time on the recombination current density J_0. The ECV profiles shown in Figure 2C,D are used to calculate the Auger contribution (using EDNA2[41]) for comparison with the total measured J_0. Figure 3A,C shows the measured total recombination and simulated Auger recombination after annealing at different temperatures for 60 min and annealing at 950 °C for different time periods, before and after a hydrogenation step by AlO_x/SiN_x + FGA or FGA only, respectively. Increasing the annealing temperature shows a significant increment in the Auger recombination (solid columns, Figure 3A). At higher annealing temperatures (1000 °C), the recombination is largely dominated by the Auger recombination, whereas at lower annealing temperatures, there is still significant room for improvement in the surface passivation. A similar trend can also be observed on the samples annealed at 950 °C for different dwell times (Figure 3C). Increasing the drive-in time shows a slight increment in the Auger recombination and also a little change in the total surface recombination (Figure 3C). Annealing in the forming gas also shows a slight effect on the total recombination (bringing the total J_0 down to similar values across different thicknesses) but little effect on the Auger recombination as the doping density is not affected (Figure 3C). This explains the similar iV_{oc} values observed after FGA for the three poly-Si thicknesses (Figure 2B).

Figure 3B,D presents sheet resistances (R_{sh}) measured by a 4PP (solid symbols, solid lines) and simulated by EDNA2 without the contribution from the poly-Si layer (open symbols, dashed lines) from the different boron spin-coated samples. The two different R_{sh} values allow us to analyze the contribution from the buried junction in comparison with the contribution from the poly-Si layer. With the drive-in temperature increasing from 850 to 1000 °C, the sheet resistances for three poly-Si thicknesses all decrease (from 300 down to 50 Ω/sq with 4PP measurements and from 1000 to ~100 Ω/sq with simulated results).

Increasing the poly-Si film thickness shows decreasing R_{sh} (4PP, Figure 3B,D), while only a little difference is observed in the EDNA2 results, revealing the strong contribution of the poly-Si layer. Meanwhile, a prolonged dwell time indicates negligible effects on the sheet resistance for different thicknesses when measured by a 4PP (Figure 3D) as R_{sh} is dominated by the high doping concentration within the poly-Si layer. On the other hand, in the simulated results from the diffused profile only (Figure 3D), a clear decrease in R_{sh} from ~700 to ~400 Ω/sq is visible (Figure 3D).

Finally, we investigate the electrical performance of the boron spin-coated poly-Si/SiO_x passivating contacts by measuring the contact resistivity using the TLM[47] and also measuring the sheet resistances to verify our previous observations. As can be seen from Figure 4, surprisingly, increasing the annealing temperatures shows an increment in the contact resistivity. This might be explained by the fact that at higher temperatures (>900 °C), the interfacial oxide possibly changes toward a more stoichiometric SiO_2 layer, that is, a denser oxide layer which likely blocks more boron diffusion into the c-Si substrate,[48,49] and also increases the electrical resistance of this interfacial layer, leading to the higher contact resistivities. Despite that, for all annealing temperatures, the contact resistivities are low and in the range of 1−10 mΩ cm^2. Figure 4 also shows the correlating sheet

https://doi.org/10.1021/acsaem.1c00550
ACS Appl. Energy Mater. 2021, 4, 4993−4999

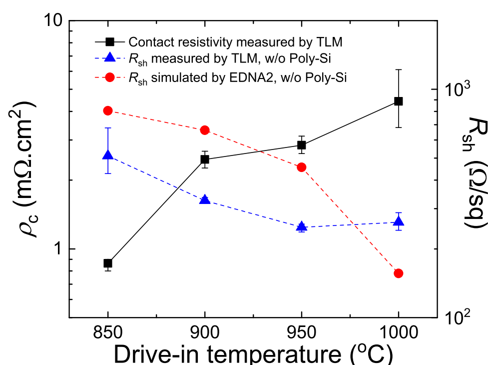

Figure 4. Contact resistivities (ρ_c, black squared symbols, solid line) of the 100 nm boron spin-on doped poly-Si/SiO_x passivating contacts formed at different annealing temperatures for 60 min, their corresponding sheet resistances (R_{sh}) measured using the TLM, and the simulated sheet resistance by EDNA2.[41] The samples were sintered in forming gas at 250 °C for 10 min before measurement.

resistances obtained from the TLM measurements (triangular symbols, dashed line) and simulated by EDNA2 (as shown in Figure 3B, re-plotted here for clearer comparisons, round symbols, dashed line). Generally, the measured and simulated sheet resistances agreed well within the accuracy of the measurement setups.

4. CONCLUSIONS

In conclusion, we have explored the impacts of drive-in temperature, drive-in dwell time, and intrinsic poly-Si thickness on the performance of boron spin-coated poly-Si passivating contacts. For all poly-Si thicknesses, an optimal annealing temperature of 950 °C for 60 min was found in terms of passivation quality. After a hydrogenation treatment by deposited AlO_x/SiN_x stacks and annealing in the forming gas, an iV_{oc} of 720 mV together with a low ρ_c of below 5 mΩ cm^2 was achieved. Prolonged annealing time shows a slight increase in iV_{oc} together with a stronger diffusion in the c-Si bulk. The poly-Si thickness presents negligible effects on the recombination studies. These results indicate the great potential of boron spin-on doping as a promising alternative doping method to fabricate high-performing poly-Si passivating contacts.

AUTHOR INFORMATION

Corresponding Authors

Thien N. Truong − *School of Engineering, The Australian National University, Canberra, Australian Capital Territory 2600, Australia;* orcid.org/0000-0002-4082-7999; Email: thien.truong@anu.edu.au

Josua Stuckelberger − *School of Engineering, The Australian National University, Canberra, Australian Capital Territory 2600, Australia*; Email: josua.stuckelberger@anu.edu.au

Authors

Zetao Ding − *School of Engineering, The Australian National University, Canberra, Australian Capital Territory 2600, Australia*

Hieu T. Nguyen − *School of Engineering, The Australian National University, Canberra, Australian Capital Territory 2600, Australia;* orcid.org/0000-0003-1667-1135

Di Yan − *Department of Electrical and Electronic Engineering, The University of Melbourne, Victoria 3010, Australia*

Xinyu Zhang − *Jinko Solar Co., Ltd, Shangrao, Jiangxi 334100, China*

Jie Yang − *Zhejiang Jinko Solar Co., Ltd, Jiaxing, Zhejiang 314416, China*

Zhao Wang − *Zhejiang Jinko Solar Co., Ltd, Jiaxing, Zhejiang 314416, China*

Peiting Zheng − *Zhejiang Jinko Solar Co., Ltd, Jiaxing, Zhejiang 314416, China*

Yimao Wan − *School of Engineering, The Australian National University, Canberra, Australian Capital Territory 2600, Australia;* orcid.org/0000-0003-2999-2464

Daniel Macdonald − *School of Engineering, The Australian National University, Canberra, Australian Capital Territory 2600, Australia*

Complete contact information is available at: https://pubs.acs.org/10.1021/acsaem.1c00550

Author Contributions

[⊥]Z.D. and T.N.T. contributed equally in this work.

Notes

The authors declare no competing financial interest.

ACKNOWLEDGMENTS

This work has been supported by the Australian Renewable Energy Agency (ARENA) through research grants RND016 and RND017. The authors acknowledge support from the Australian National Fabrication Facility (ANFF)−ACT Node and the Department of Electronic Materials Engineering, The Australian National University. H.T.N. and J.S. acknowledge the fellowship supports from the Australian Centre for Advanced Photovoltaics (ACAP).

REFERENCES

(1) Green, M. A. Photovoltaic Technology and Visions for the Future. *Prog. Energy* **2019**, *1*, 013001.
(2) Green, M. A. How Did Solar Cells Get So Cheap? *Joule* **2019**, *3*, 631−633.
(3) Green, M. A. Tracking Solar Cell Conversion Efficiency. *Nat. Rev. Phys.* **2020**, *2*, 172−173.
(4) Richter, A.; Hermle, M.; Glunz, S. W. Reassessment of the Limiting Efficiency for Crystalline Silicon Solar Cells. *IEEE J. Photovoltaics* **2013**, *3*, 1184−1191.
(5) Melskens, J.; Van De Loo, B. W. H.; Macco, B.; Black, L. E.; Smit, S.; Kessels, W. M. M. Passivating Contacts for Crystalline Silicon Solar Cells: From Concepts and Materials to Prospects. *IEEE J. Photovoltaics* **2018**, *8*, 373−388.
(6) Richter, A.; Glunz, S. W.; Werner, F.; Schmidt, J.; Cuevas, A. Improved Quantitative Description of Auger Recombination in Crystalline Silicon. *Phys. Rev. B: Condens. Matter Mater. Phys.* **2012**, *86*, 165202.
(7) Battaglia, C.; Cuevas, A.; De Wolf, S. High-Efficiency Crystalline Silicon Solar Cells: Status and Perspectives. *Energy Environ. Sci.* **2016**, *9*, 1552−1576.
(8) Haase, F.; Hollemann, C.; Schäfer, S.; Merkle, A.; Rienäcker, M.; Krügener, J.; Brendel, R.; Peibst, R. Laser Contact Openings for Local Poly-Si-Metal Contacts Enabling 26.1%-Efficient POLO-IBC Solar Cells. *Sol. Energy Mater. Sol. Cells* **2018**, *186*, 184−193.
(9) Richter, A.; Benick, J.; Müller, R.; Feldmann, F.; Reichel, C.; Hermle, M.; Glunz, S. W. Tunnel Oxide Passivating Electron Contacts as Full-Area Rear Emitter of High-Efficiency p-Type Silicon Solar Cells. *Prog. Photovoltaics Res. Appl.* **2018**, *26*, 579−586.
(10) Yan, D.; Cuevas, A.; Michel, J. I.; Zhang, C.; Wan, Y.; Zhang, X.; Bullock, J. Polysilicon Passivated Junctions: The next Technology for Silicon Solar Cells? *Joule* **2021**, *5*, 811.

https://doi.org/10.1021/acsaem.1c00550
ACS Appl. Energy Mater. 2021, 4, 4993−4999

(11) Liu, C.; Chen, D.; Chen, Y.; Ling, Y.; Zou, Y.; Wang, Y.; Gong, J.; Feng, Z.; Altermatt, P. P.; Verlinden, P. J. Industrial TOPCon Solar Cells on N-Type Quasi-Mono Si Wafers with Efficiencies above 23%. *Sol. Energy Mater. Sol. Cells* **2020**, *215*, 110690.

(12) Messmer, C.; Fell, A.; Feldmann, F.; Wohrle, N.; Schon, J.; Hermle, M. Efficiency Roadmap for Evolutionary Upgrades of PERC Solar Cells by TOPCon: Impact of Parasitic Absorption. *IEEE J. Photovoltaics* **2020**, *10*, 335−342.

(13) Chen, D.; Chen, Y.; Wang, Z.; Gong, J.; Liu, C.; Zou, Y.; He, Y.; Wang, Y.; Yuan, L.; Lin, W. 24.58% Total Area Efficiency of Screen-Printed, Large Area Industrial Silicon Solar Cells with the Tunnel Oxide Passivated Contacts (i-TOPCon) Design. *Sol. Energy Mater. Sol. Cells* **2020**, *206*, 110258.

(14) Chen, Y.; Chen, D.; Liu, C.; Wang, Z.; Zou, Y.; He, Y.; Wang, Y.; Yuan, L.; Gong, J.; Lin, W. Mass Production of Industrial Tunnel Oxide Passivated Contacts (I-TOPCon) Silicon Solar Cells with Average Efficiency over 23% and Modules over 345 W. *Prog. Photovoltaics Res. Appl.* **2019**, *27*, 827.

(15) Yan, D.; Cuevas, A.; Phang, S. P.; Wan, Y.; Macdonald, D. 23% Efficient P-Type Crystalline Silicon Solar Cells with Hole-Selective Passivating Contacts Based on Physical Vapor Deposition of Doped Silicon Films. *Appl. Phys. Lett.* **2018**, *113*, 061603.

(16) Feldmann, F.; Simon, M.; Bivour, M.; Reichel, C.; Hermle, M.; Glunz, S. W. Carrier-Selective Contacts for Si Solar Cells. *Appl. Phys. Lett.* **2014**, *104*, 181105.

(17) Nemeth, B.; Young, D. L.; Page, M. R.; Lasalvia, V.; Johnston, S.; Reedy, R.; Stradins, P. Polycrystalline Silicon Passivated Tunneling Contacts for High Efficiency Silicon Solar Cells. *J. Mater. Res.* **2016**, *31*, 671−681.

(18) Stuckelberger, J.; Nogay, G.; Wyss, P.; Jeangros, Q.; Allebé, C.; Debrot, F.; Niquille, X.; Ledinsky, M.; Fejfar, A.; Despeisse, M.; Haug, F.-J.; Löper, P.; Ballif, C. Passivating Electron Contact Based on Highly Crystalline Nanostructured Silicon Oxide Layers for Silicon Solar Cells. *Sol. Energy Mater. Sol. Cells* **2016**, *158*, 2−10.

(19) Stuckelberger, J.; Loper, P.; Ballif, C.; Nogay, G.; Wyss, P.; Ingenito, A.; Allebe, C.; Horzel, J.; Kamino, B. A.; Despeisse, M.; Haug, F.-J. Recombination Analysis of Phosphorus-Doped Nanostructured Silicon Oxide Passivating Electron Contacts for Silicon Solar Cells. *IEEE J. Photovoltaics* **2018**, *8*, 389−396.

(20) Truong, T. N.; Yan, D.; Nguyen, C. T.; Kho, T.; Guthrey, H.; Seidel, J.; Al-Jassim, M.; Cuevas, A.; Macdonald, D.; Nguyen, H. T. Morphology, Microstructure, and Doping Behaviour: A Comparison between Different Deposition Methods for Poly-Si/SiOx Passivating Contacts. *Prog. Photovoltaics Res. Appl.* **2021**, DOI: 10.1002/pip.3411.

(21) Fong, K. C.; Kho, T. C.; Liang, W.; Chong, T. K.; Ernst, M.; Walter, D.; Stocks, M.; Franklin, E.; McIntosh, K.; Blakers, A. Phosphorus Diffused LPCVD Polysilicon Passivated Contacts with In-Situ Low Pressure Oxidation. *Sol. Energy Mater. Sol. Cells* **2018**, *186*, 236−242.

(22) Stodolny, M. K.; Lenes, M.; Wu, Y.; Janssen, G. J. M.; Romijn, I. G.; Luchies, J. R. M.; Geerligs, L. J. N-Type Polysilicon Passivating Contact for Industrial Bifacial n-Type Solar Cells. *Sol. Energy Mater. Sol. Cells* **2016**, *158*, 24−28.

(23) Feldmann, F.; Müller, R.; Reichel, C.; Hermle, M. Ion Implantation into Amorphous Si Layers to Form Carrier-Selective Contacts for Si Solar Cells. *Phys. Status Solidi RRL* **2014**, *08*, 767−770.

(24) Reichel, C.; Feldmann, F.; Müller, R.; Reedy, R. C.; Lee, B. G.; Young, D. L.; Stradins, P.; Hermle, M.; Glunz, S. W. Tunnel Oxide Passivated Contacts Formed by Ion Implantation for Applications in Silicon Solar Cells. *J. Appl. Phys.* **2015**, *118*, 205701.

(25) Truong, T. N.; Yan, D.; Chen, W.; Wang, W.; Guthrey, H.; Al-Jassim, M.; Cuevas, A.; Macdonald, D.; Nguyen, H. T. Deposition Pressure Dependent Structural and Optoelectronic Properties of Ex-Situ Boron-Doped Poly-Si/SiOx Passivating Contacts Based on Sputtered Silicon. *Sol. Energy Mater. Sol. Cells* **2020**, *215*, 110602.

(26) Chen, W.; Truong, T. N.; Nguyen, H. T.; Samundsett, C.; Phang, S. P.; MacDonald, D.; Cuevas, A.; Zhou, L.; Wan, Y.; Yan, D. Influence of PECVD Deposition Temperature on Phosphorus Doped Poly-Silicon Passivating Contacts. *Sol. Energy Mater. Sol. Cells* **2020**, *206*, 110348.

(27) Scardera, G.; Inns, D.; Wang, G.; Dugan, S.; Dee, J.; Dang, T.; Bendimerad, K.; Lemmi, F.; Antoniadis, H. All-Screen-Printed Dopant Paste Interdigitated Back Contact Solar Cell. *Energy Procedia* **2015**, *77*, 271−278.

(28) Recart, F.; Freire, I.; Pérez, L.; Lago-Aurrekoetxea, R.; Jimeno, J. C.; Bueno, G. Screen Printed Boron Emitters for Solar Cells. *Sol. Energy Mater. Sol. Cells* **2007**, *91*, 897−902.

(29) Zagozdzon-Wosik, W.; Grabiec, P. B.; Lux, G. Silicon Doping from Phosphorus Spin-on Dopant Sources in Proximity Rapid Thermal Diffusion. *J. Appl. Phys.* **1994**, *75*, 337−344.

(30) Mathiot, D.; Lachiq, A.; Slaoui, A.; Noël, S.; Muller, J. C.; Dubois, C. Phosphorus Diffusion from a Spin-on Doped Glass (SOD) Source during Rapid Thermal Annealing. *Mater. Sci. Semicond. Process.* **1998**, *1*, 231−236.

(31) Ding, Z.; Yan, D.; Stuckelberger, J.; Phang, S. P.; Chen, W.; Samundsett, C.; Yang, J.; Wang, Z.; Zheng, P.; Zhang, X.; Wan, Y.; Macdonald, D. Phosphorus-Doped Polycrystalline Silicon Passivating Contacts via Spin-on Doping. *Sol. Energy Mater. Sol. Cells* **2021**, *221*, 110902.

(32) Young, D. L.; Lee, B. G.; Fogel, D.; Nemeth, W.; LaSalvia, V.; Theingi, S.; Page, M.; Young, M.; Perkins, C.; Stradins, P. Gallium-Doped Poly-Si:Ga/SiO2 Passivated Emitters to n-Cz Wafers with IVoc >730 MV. *IEEE J. Photovoltaics* **2017**, *7*, 1640−1645.

(33) Teh, S. T.; Chuah, D. G. S. Diffusion Profile of Spin-on Dopant in Silicon Substrate. *Sol. Energy Mater.* **1989**, *19*, 237−247.

(34) Hartiti, B.; Slaoui, A.; Muller, J. C.; Stuck, R.; Siffert, P. Phosphorus Diffusion into Silicon from a Spin-on Source Using Rapid Thermal Processing. *J. Appl. Phys.* **1992**, *71*, 5474−5478.

(35) Yang, X.; Kang, J.; Liu, W.; Zhang, X.; De Wolf, S. Solution-Doped Polysilicon Passivating Contacts for Silicon Solar Cells. *ACS Appl. Mater. Interfaces* **2021**, *13*, 8455.

(36) Hawkinson, T. E.; Korpela, D. B. Chemical Hazards in Semiconductor Operations. *Semiconductor Safety Handbook*; Elsevier, 1998; pp 187−203.

(37) Ryssel, H.; Haberger, K. Ion implantation: safety and radiation considerations. *Ion Implantation Science and Technology*; Elsevier, 1984; pp 603−627.

(38) Kiaee, Z.; Reichel, C.; Keding, R.; Nazarzadeh, M.; Lohmann, R.; Feldmann, F.; Jahn, M.; Huyeng, D. J.; Hermle, M.; Clement, F. Inkjet-Printing of Phosphorus and Boron Dopant Sources for Tunnel Oxide Passivating Contacts. *36th European Photovoltaic Solar Energy Conference and Exhibition*, 2019; pp 187−191.

(39) Kiaee, Z.; Reichel, C.; Hussain, Z.; Nazarzadeh, M.; Huyeng, J. D.; Clement, F.; Hermle, M.; Keding, R. Inkjet Printing of Phosphorus Dopant Sources for Doping Poly-Silicon in Solar Cells with Passivating Contacts. *Sol. Energy Mater. Sol. Cells* **2021**, *222*, 110926.

(40) Kane, D. E.; Swanson, R. M. Measurement of the Emitter Saturation Current by a Contactless Photoconductivity Decay Method. *18th IEEE Photovoltaic Specialists Conference*; 1985; pp 578−583.

(41) PVLighthouse EDNA 2. https://www2.pvlighthouse.com.au/calculators/EDNA2/EDNA2.aspx (accessed Nov 9, 2020).

(42) Truong, T. N.; Yan, D.; Chen, W.; Tebyetekerwa, M.; Young, M.; Al-Jassim, M.; Cuevas, A.; Macdonald, D.; Nguyen, H. T. Hydrogenation Mechanisms of Poly-Si/SiO x Passivating Contacts by Different Capping Layers. *Sol. RRL* **2019**, *4*, 1900476.

(43) Truong, T. N.; Yan, D.; Samundsett, C.; Liu, A.; Harvey, S. P.; Young, M.; Ding, Z.; Tebyetekerwa, M.; Kremer, F.; Al-Jassim, M.; Cuevas, A.; Macdonald, D.; Nguyen, H. T. Hydrogen-Assisted Defect Engineering of Doped Poly-Si Films for Passivating Contact Solar Cells. *ACS Appl. Energy Mater.* **2019**, *2*, 8783−8791.

(44) Truong, T. N.; Yan, D.; Samundsett, C.; Basnet, R.; Tebyetekerwa, M.; Li, L.; Kremer, F.; Cuevas, A.; Macdonald, D.; Nguyen, H. T. Hydrogenation of Phosphorus-Doped Polycrystalline Silicon Films for Passivating Contact Solar Cells. *ACS Appl. Mater. Interfaces* **2019**, *11*, 5554−5560.

https://doi.org/10.1021/acsaem.1c00550
ACS Appl. Energy Mater. 2021, 4, 4993−4999

(45) Feldmann, F.; Bivour, M.; Reichel, C.; Steinkemper, H.; Hermle, M.; Glunz, S. W. Tunnel Oxide Passivated Contacts as an Alternative to Partial Rear Contacts. *Sol. Energy Mater. Sol. Cells* **2014**, *131*, 46−50.
(46) van de Loo, B. W. H.; Macco, B.; Schnabel, M.; Stodolny, M. K.; Mewe, A. A.; Young, D. L.; Nemeth, W.; Stradins, P.; Kessels, W. M. M. On the Hydrogenation of Poly-Si Passivating Contacts by Al2O3 and SiN Thin Films. *Sol. Energy Mater. Sol. Cells* **2020**, *215*, 110592.
(47) Berger, H. H. Contact Resistance and Contact Resistivity. *J. Electrochem. Soc.* **1972**, *119*, 507−514.
(48) Khalilov, U.; Pourtois, G.; Van Duin, A. C. T.; Neyts, E. C. On the c -Si| a -SiO 2 Interface in Hyperthermal Si Oxidation at Room Temperature. *J. Phys. Chem. C* **2012**, *116*, 21856−21863.
(49) Stuckelberger, J. *Transparent Passivating Contacts for Front Side Application in Crystalline Silicon Solar Cells*; EPFL: Lausanne, 2018.

https://doi.org/10.1021/acsaem.1c00550
ACS Appl. Energy Mater. 2021, 4, 4993−4999